

Observation of the $\tilde{A}-\tilde{X}$ Electronic Transitions of Cyclopentyl and Cyclohexyl Peroxy Radicals via Cavity Ringdown Spectroscopy

Phillip S. Thomas, Rabi Chhantyal-Pun, and Terry A. Miller*

Department of Chemistry, The Ohio State University, 120 W. 18th Avenue, Columbus Ohio 43210

Received: August 6, 2009; Revised Manuscript Received: September 30, 2009

The $\tilde{A}-\tilde{X}$ electronic absorption spectra of cyclopentyl, cyclohexyl, and cyclohexyl-*d*₁₁ peroxy radicals have been recorded at room temperature by cavity ringdown spectroscopy. By comparing the experimental spectra with predictions from ab initio and density functional calculations, we have assigned the band origins and vibrational structure of each of these species. The spectrum of cyclopentyl peroxy is interpreted primarily in terms of two overlapping gauche conformers, while that of cyclohexyl peroxy appears to be a superposition of axially and equatorially substituted gauche conformers, both based on the chair conformation of cyclohexane. Expectations from calculated Boltzmann factors indicate comparable populations for cis-conformers; however, no bands uniquely assignable to cis-conformers of either peroxy can be identified. Plausible assignments for cis-conformers are considered, and possible explanations for their absence are offered, including specifically lower oscillator strengths than for the gauche conformers. Mode mixing appears to be responsible for the appearance of multiple vibrations with COO bending character for both peroxies, particularly for cyclohexyl peroxy.

1. Introduction

Organic peroxy radicals (RO₂•, R = alkyl) are cardinal intermediates in hydrocarbon oxidation mechanisms. Addition of O₂ to an alkyl radical to form an organic peroxy radical is an early, and essential, step in a plethora of reaction sequences that take place in low-temperature combustion.^{1–4} The importance of the alkyl radical-oxygen addition arises from its competitive nature with radical self- and cross-reactions which are ultimately soot forming.⁵ Understanding the mechanisms of RO₂• formation and reaction is essential for fuel development and for optimizing the efficiency of combustion engines.⁶ This point is emphasized for cyclopentyl and cyclohexyl peroxy radicals, as their parent alkanes are becoming increasingly common as constituents of alternative fuels.^{7,8} Unraveling the oxidation mechanisms of cyclopentane^{9–15} and cyclohexane^{13,15–26} has already been the focus of several experimental studies, particularly the latter, as cyclohexane combustion has been implicated in the production of benzene, a precursor to soot and an environmental hazard.^{22,27} Kinetic models^{28–30} designed for assessing product ratios from combustion of real fuels frequently employ rate constants derived from cyclohexane oxidation data to represent the naphthene (cyclic alkane) component.^{31–33}

Peroxy radicals derived from hydrocarbons are also known to play critical roles in atmospheric oxidation processes^{34–36} in both polluted (i.e., NO_x-containing) and clean environments. In the former, RO₂• participates with NO and NO₂ in reaction pathways that are favorable to O₃ accumulation;^{3,37} in the latter, organic peroxy radicals are the precursors to a variety of oxygen-containing volatile organic compounds (VOCs),^{22,35} some of which may be implicated in acid rain formation. An example of a reaction in the clean troposphere is that between an alkyl peroxy radical and HO₂, an important atmospheric intermediate:¹⁰



Kinetic behavior for reaction 1 strongly depends on the R group involved. For example, rate constants are $\approx 3\times$ higher and exhibit a $\approx 1.5\times$ steeper negative temperature dependence for cyclopentyl and cyclohexyl peroxies as compared to methyl peroxy.¹⁰ It is therefore indispensable to gain a clear understanding of the structural principles which govern the reactivity of peroxy radicals, to which end structure-specific diagnostics are instrumental. In this report, we present the $\tilde{A}-\tilde{X}$ cavity ringdown (CRDS) spectra of cyclopentyl and cyclohexyl peroxy radicals. The observed spectra represent potential diagnostics that clearly distinguish between the two species, and further distinction is made between some of the conformers of cyclohexyl peroxy.

Previous experimental efforts have already yielded the $\tilde{B}-\tilde{X}$ absorption spectra of cyclopentyl^{10,14} and cyclohexyl^{19,20,38} peroxies, both of which consist of broad, featureless absorptions centered around 250 nm with widths (fwhm) of ~ 40 nm. Cyclopentyl³⁹ and cyclohexyl^{39,40} peroxies have also been investigated via solution-phase EPR spectroscopy, the latter most recently by DiLabio, Ingold, and Walton (DIW), who attempted to observe distinct EPR signals for the axial and equatorial conformers.⁴⁰ Although their calculations predicted that the most stable axial and equatorial forms of cyclohexyl peroxy are close in energy, DIW were able to observe only one signal, probably due to similar hyperfine parameters for the two species. Potential energy curves computed for the O–O–C–H torsional coordinate featured two distinct types of minima for each (axial, equatorial) conformer, with O–O–C–H dihedral angles of 180° and ca. $\pm 45^\circ$. The latter types (dubbed “gauche” in this study, vide infra) were predicted to be more stable than the former (“cis”) forms.⁴⁰

Generally, the electronic structure of RO₂• molecules bears analogy to that of O₂, as the lowest few electronic transitions are dominated by excitations localized on the dioxygen moiety.⁴¹ The $\tilde{B}-\tilde{X}$ system of alkyl peroxies occurs in the UV (c.f.

* Corresponding author. E-mail: tamiller@chemistry.ohio-state.edu.

Schumann–Runge absorption of O_2); this transition has found widespread application in kinetic studies by virtue of its large oscillator strength. However, the $\tilde{B}-\tilde{X}$ transition is not useful for distinguishing among different RO_2 species nor for structure determination, as facile dissociation on the \tilde{B} state surface⁴² leads to broad, featureless absorption profiles.³⁷ In contrast, the \tilde{A} state of organic peroxy radicals is bound and has been exploited not only to distinguish between peroxy radicals with different alkyl substituents but also between isomers and conformers of a given peroxy radical.^{43–48} Since the near-IR $\tilde{A}-\tilde{X}$ manifold of organic peroxy radicals retains much of the forbidden character of the related $a^1\Delta_g \leftarrow X^3\Sigma_g^-$ system of O_2 ,⁴⁹ observation of this transition requires a sensitive spectroscopic technique. Cavity ringdown spectroscopy is well-suited for this purpose^{43,50} and has already proven fruitful for a number of hydrocarbon-based peroxy radicals.^{44,46–48,51–53}

Following previous observations of isomers and conformers of straight-chain alkyl peroxy radicals,^{44,46–48,51} we now consider cyclic species, beginning with cyclopentyl and cyclohexyl peroxies. There are significant differences between the structure of the open-chain and cyclic alkyl peroxy, and these studies for the first time show how these structural differences are reflected in their spectra. This work represents the first attempts to distinguish between axial and equatorial conformers of a peroxy radical on the basis of an electronic transition. We therefore expect that $\tilde{A}-\tilde{X}$ electronic spectral profiles of cyclic systems will vary with ring conformation and with orientation of the O_2 fragment with respect to the ring. Herein, we report the $\tilde{A}-\tilde{X}$ electronic absorption spectra of cyclopentyl and cyclohexyl peroxy radicals, along with the spectral analysis in terms of their conformers and vibrations.

2. Features of Peroxy Radical Spectra

A thorough review of cavity ringdown data and trends from $\tilde{A}-\tilde{X}$ electronic spectra of organic peroxy radicals has recently been published.⁵⁴ Here we briefly review some key features. The O_2 moiety is the chromophore of the $\tilde{A}-\tilde{X}$ transition; accordingly, geometric changes leading to observable vibrational structure occur in the vicinity of the oxygen atoms. Peroxy $\tilde{A}-\tilde{X}$ spectra therefore typically exhibit moderately strong progressions in $O-O$ stretching vibrations ($870-1000\text{ cm}^{-1}$) and weaker progressions in COO bending modes ($350-600\text{ cm}^{-1}$), with the latter being somewhat variable in intensity. Additionally, organic peroxy radicals possess a low frequency ($<200\text{ cm}^{-1}$) $O-O-C-H$ torsional vibration which often has several quanta populated at room temperature and contributes to sequence band structure.⁵⁴

For open chain alkyl peroxy radicals, it is known that the number of possible isomers and conformers increases rapidly with chain length, from a single minimum geometry for methyl peroxy,^{51,55} to approximately 170 isomers/conformers for pentyl peroxy.⁴⁸ In the case of small cyclic alkanes (≤ 6 carbon atoms) the situation is simplified considerably. Using the structure of cyclohexane as a reference,⁵⁶ cyclohexyl peroxy should exist in chair and twist-boat forms, but the latter is predicted to lie $>2000\text{ cm}^{-1}$ above the former²⁴ and will not be thermally populated at ambient temperature. From the potential curves of DIW,⁴⁰ we expect axial and equatorial substitution of the chair ring geometry, with two types of minima distinguished by the $O-O-C-H$ dihedral angle for each. For $D(O-O-C-H) = 180^\circ$, the O_2 fragment is oriented toward the ring; this geometry we dub the “cis”; the two enantiomeric minima with $D(O-O-C-H) \approx \pm 45^\circ$ are dubbed “gauche”. The “trans” geometry, at $D(O-O-C-H) = 0^\circ$, is not a minimum on the potential energy

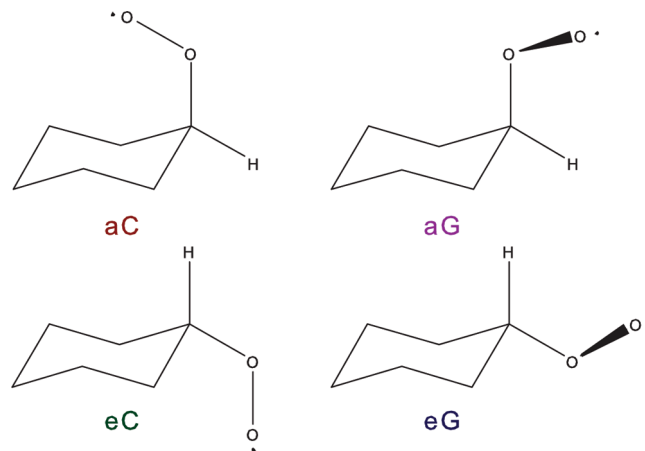


Figure 1. Conformers of cyclohexyl peroxy. Each gauche conformer exists as mirror image pairs.

surface but rather a transition state connecting the gauche enantiomers. The four expected conformers of chair cyclohexyl peroxy are thus axial cis (aC), axial gauche (aG), equatorial cis (eC), and equatorial gauche (eG), as shown in Figure 1.

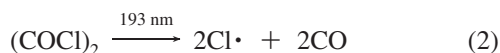
The potential energy surface of cyclopentyl peroxy is more difficult to rationalize simply by chemical intuition. Cyclopentane has a very flat ring-bending potential, such that interconversion between its two stable conformers, the “envelope” and “half-chair”, occurs via nearly barrierless pseudorotation.^{57–62} A survey of some monosubstituted cyclopentanes reveals that the ring-puckering potential, in comparison to cyclopentane itself, can be significantly altered depending on the substituent. For chlorocyclopentane,^{63,64} bromocyclopentane,^{65–67} cyanocyclopentane,^{68,69} and cyclopentylacetylene,⁷⁰ the rings adopt the envelope conformation with axial/equatorial substitution at the bridge position, where the axial form is more stable for the two cyclopentyl halides and the equatorial conformation is preferred for cyanocyclopentane and cyclopentylacetylene. Another species, cyclopentylsilane,⁷¹ is believed to possess a third type of low-lying conformer having a “twisted” ring geometry. We therefore expect conformers differing in ring geometry and in orientation of the $O-O$ moiety for cyclopentyl peroxy; these will be identified on the basis of ab initio and density functional theory (DFT) calculations, as described in Section 5.1.

3. Experimental Section

3.1. Experimental Apparatus. Our cavity ringdown apparatus used for detection of peroxy radical transitions in the NIR is similar to the one described previously.⁴⁷ The second harmonic of a 20 Hz pulsed Nd:YAG (Spectra Physics, Quanta-Ray Pro 270) was used to pump a dye laser (Sirah, Precision-Scan) to yield 50–110 mJ/pulse visible light over the wavelength range 669–570 nm. The laser dyes utilized were: DCM, Rhodamine 101, Rhodamine B, and Pyrromethene 597 (Exciton). Output from the dye laser was focused into a 70 cm single-pass Raman cell charged with 300–325 psi of H_2 . The desired second Stokes component ($6630-9230\text{ cm}^{-1}$; 1–3 mJ/pulse) of the stimulated Raman scattered radiation was isolated via several long pass filters (Corion, LL-1000-F; Newport, 1000 nm LP); the resultant NIR light was focused into the ringdown cell by two 2 m focal lenses. The ringdown cell is 55 cm in length and is terminated by two highly reflective mirrors (Los Gatos Research; $1.4\ \mu\text{m}$, $R \geq 99.995\%$; $1.3\ \mu\text{m}$, $\geq 99.995\%$; $1.2\ \mu\text{m}$, $\geq 99.995\%$; $1.064\ \mu\text{m}$, $\geq 99.999\%$). The inner 20 cm portion of the cell is outfitted with sample gas inlets on either end, a central vacuum port, and two rectangular UV-grade quartz

photolysis windows. Protection of the mirrors from corrosion and chemical deposits is accomplished by a steady flow of nitrogen at 10 cm³/min. Similarly, the quartz photolysis windows were purged by nitrogen at 250 cm³/min to inhibit soot buildup during photolysis. Upon leaving the cell, the NIR light is focused by a 2.5 cm focal lens onto an amplified InGaAs photodiode detector (Thorlabs, PDA400); this signal is recorded via a 12-bit digitizing card (Measurement Computing). Photolysis of precursor molecules was attained by an excimer laser (Lambda-Physik, LPX120i) operating at 193 nm (ArF). Pulses of 120–200 mJ were focused via a spherical lens and a cylindrical lens into a rectangular shape 13 × 0.5 cm. This beam was focused into the ringdown cell through the quartz windows in such a manner to yield maximum overlap of the photolysis beam and NIR probe beam. The delay between the excimer pulse and the probe pulse of 5 μs was long enough for peroxy radicals to form but not long enough for them to be consumed by reactions or to be pumped out of the cell. Spectra were acquired by averaging 20–40 measurements at each wavelength, and instrumental step sizes were on the order of ~0.5 cm⁻¹. In order to remove spectral artifacts arising from water or precursor absorptions or from cavity structure, a background trace (without photolysis) was concurrently acquired and subsequently subtracted from the trace resulting from photolysis. Spectra were calibrated by comparison of observed water signals with those in the HITRAN 2004 database.⁷² Uncertainties in positions of band maxima are estimated at ±2 cm⁻¹; absolute frequencies of band origins are expected to be within ±10 cm⁻¹ due to overlap of multiple conformer origins. Operation of the lasers and data acquisition was achieved by PC-based Labview software.

3.2. Peroxy Radical Generation. Organic peroxy radicals are produced by addition of molecular oxygen to an alkyl radical.⁴ The alkyl radical can be generated either by photolysis of an appropriate alkyl halide⁷³ or by H-atom abstraction from an alkane by atomic chlorine. In the latter method, chlorine atoms are obtained in high yield by oxalyl chloride photolysis.⁷⁴ Initially, we investigated cyclohexyl bromide as a precursor for cyclohexyl radicals, but the low equilibrium vapor pressure of this precursor led to very low (<5 ppm) peroxy signals. In contrast, a much stronger peroxy signal was obtained using the chlorine atom reaction with cyclopentane or cyclohexane in the alkyl radical-forming step:



Here, M represents a third body. For each experiment, a stream of N₂ with a backing pressure of ~30 psi was bubbled through a liquid sample of cyclopentane (Aldrich, ≥99%), cyclohexane (Fisher, ACS grade), or cyclohexane-*d*₁₂ (Cambridge Isotope Laboratories, 99.5%). Oxalyl chloride (Aldrich, 98%) was prepared as a dilute mixture in N₂ with a concentration of 0.2–1.5%. The concentration of oxalyl chloride was determined by measuring the excimer laser absorption by a known pressure of the oxalyl chloride mixture, using the absorption cross-section of oxalyl chloride ($\sigma = 3.8 \times 10^{-18}$ cm² at 193 nm⁷⁵). The alkane/N₂ and oxalyl chloride/N₂ mixtures were mixed with N₂ and O₂ prior to entering the ringdown cell, where

photolysis and measurement are subsequently performed. For cyclohexyl peroxy, typical reaction mixtures were prepared with [N₂] = 9.0 Torr, [O₂] = 10.5 Torr, [C₆H₁₂/N₂] = 1.2 Torr, and [(COCl)₂] (1.76% in N₂) = 2.0 Torr; a total pressure of 54 Torr was obtained by adjusting the size of the gas outlet aperture to reduce the rate at which the cell is pumped out. For cyclopentyl peroxy, a representative reaction mixture contained [N₂] = 9.0 Torr, [O₂] = 10.7 Torr, [C₅H₁₀/N₂] = 0.7 Torr, and [(COCl)₂] (0.25% in N₂) = 10.2 Torr; the pump rate was reduced to yield a total pressure of 95 Torr. Some variation in gas mixture composition was necessary to obtain spectra with good signal-to-noise ratios. In the 6800–7400 cm⁻¹ and 8200–8600 cm⁻¹ regions of the spectrum, intense vibrational bands of the C₅H₁₀ and C₆H₁₂ precursors engendered higher noise in the difference traces; in these regions we obtained better signal-to-noise (but lower absolute absorption) by reducing the total hydrocarbon pressure by a factor of 2–3. Soot formation on the cell photolysis window was also more problematic for these molecules than for smaller alkyl peroxies in earlier experiments. Over the course of the experiments (~6 months), we made several modifications to our CRDS apparatus (improved vacuum system, addition of a photolysis window purge); the representative conditions listed above are based on the modified apparatus. For these reasons, optimal (best S/N) conditions varied over the course of the experiments. In order to reliably compare the intensities of spectral features obtained under different conditions across the spectrum, each portion of the spectrum was overlapped with adjacent portions. We then scaled the intensities of each region so that the intensities in the overlapped portions were consistent.

4. Quantum Chemical Calculations

In order to facilitate assignment of spectroscopic features, quantum chemical calculations were performed on the conformers of cyclopentyl and cyclohexyl peroxies using the Gaussian 03W program suite.⁷⁶ Previous studies involving saturated organic peroxy radicals have shown that the G2 method predicts $\tilde{\text{A}}-\tilde{\text{X}}$ transition energies to an accuracy of a few tens of wavenumbers.⁵⁴ Oscillator strengths for the electronic transitions were computed at the UCIS/6-31G(d) and TD-B3LYP/cc-pVDZ levels using the UMP2/6-31G(d) $\tilde{\text{X}}$ state equilibrium structures obtained within the G2 calculations. Geometry optimizations and harmonic frequencies were also computed at the UB3LYP/cc-pVDZ level, as these vibrational frequencies are expected to be more accurate than those calculated at the UHF/6-31G(d) level within the G2 routine.^{24,77} Cartesian coordinates and absolute energies for optimized structures are included in Supporting Information.

For the purpose of qualitatively predicting band origin profiles of each conformer of cyclopentyl and cyclohexyl peroxies, hot sequence band simulations were accomplished. Vibrational energy levels defined by B3LYP scaled ($\times 0.970$ ⁷⁸) harmonic frequencies were calculated for each mode in the $\tilde{\text{X}}$ and $\tilde{\text{A}}$ electronic states. Assuming 298 K equilibrium Boltzmann populations, transitions were permitted from all $\tilde{\text{X}}$ state vibrational levels having Boltzmann weights ≥ 1% that of the zero level for each conformer, or from all vibrational levels with energies ≤ 950 cm⁻¹ above the zero level. Transitions to $\tilde{\text{A}}$ state levels were governed by the selection rule $\Delta\nu = 0$, which holds in the limit of identical $\tilde{\text{X}}$ and $\tilde{\text{A}}$ state potentials which are not displaced relative to one another. In this limit transitions such as 51₁⁺ and 51₂⁺ (but not 51₁⁰) are represented in the simulations; relative intensities of the allowed transitions are given simply by the Boltzmann weights of the initial ($\tilde{\text{X}}$ state) levels. All

TABLE 1: Degeneracy Numbers, Relative Energies, Origin Frequencies (cm⁻¹), and Boltzmann Weights for Conformers of Cyclopentyl and Cyclohexyl Peroxy Radicals^c

conformer	g	B3LYP/cc-pVDZ					G2				
		E		T_{00}	w	shift $\Delta(\text{H-D})$	E		T_{00}	w	expt T_{00}
		\tilde{X}	\tilde{A}				\tilde{X}	\tilde{A}			
C₅H₉O₂											
C	2	0	7776	7776	2.00		0	7645	7645	2.00	
G ₁ T ₂	2	-213	7371	7584	5.60		-242	7218	7460	6.43	7461
G ₁ G ₂	2	-80	7511	7591	2.94		-118	^a	7467 ^a	3.54	(7481) ^b
C₆H₁₁O₂											
eC	1	0	7770	7770	1.00	-11	0	7751	7751	1.00	
aC	1	734	7904	7170	0.03	-19	915	8186	7271	0.01	
eG	2	-8	7591	7599	2.08	-3	-104	7443	7547	3.30	7538
aG	2	72	7603	7531	1.41	0	-30	7428	7458	2.31	7470

^a T_{00} estimated from G₁G₂ B3LYP energies and G₁T₂ G2 energy. See text for details. ^b Tentative assignment, G₁G₂ origin overlaps the more intense G₁T₂ conformer origin. ^c Relative energies have been ZPVE corrected. Isotope shifts (cm⁻¹) for the band origins of cyclohexyl peroxy conformers are listed.

combination sequence bands permitted under the constraints stated above were also included in the simulations. For comparison with experimental spectra the calculated sequence band envelopes were shifted to place the band origins at the values predicted by G2 theory.

We also undertook Franck–Condon simulations in order to help assign the vibrational structure present in each spectrum. Animation of the normal modes for the two electronic states reveals that a number of the vibrations change upon electronic excitation (Duschinsky mixing⁷⁹). For the purpose of computing multidimensional Franck–Condon factors with the inclusion of Duschinsky rotation, we used MolFC,⁸⁰ a program developed and distributed by Borrelli and Peluso.⁸¹ Geometries and force constant matrices used as input were computed at the B3LYP/cc-pVDZ level of theory. Simulations were performed in the limit of cold (0 K) absorption. For C₅H₉O₂ and C₆H₁₁O₂, Franck–Condon factors were computed for the 23 vibrational modes of lowest frequency. The highest \tilde{A} state vibrational level for which Franck–Condon factors were calculated was $\nu_{\text{max}} = 2$ for the 9 lowest modes and $\nu_{\text{max}} = 1$ for the remaining 14 modes. As an exception, the C conformer of cyclopentyl peroxy possesses a progression in the lowest frequency (ring puckering) mode; we therefore chose $\nu_{\text{max}} = 4$ for this vibration for this conformer only. For C₆D₁₁O₂, isotope shifts resulted in a greater portion of the total number of vibrations falling in the energy range of our experiments; here, we included $\nu_{\text{max}} = 1$ for the 27 lowest frequency modes. The lowest frequency ring bending vibration of eC C₆D₁₁O₂ was found to be mildly excited in a preliminary calculation, so we set $\nu_{\text{max}} = 2$ for this mode only.

For comparison of the simulated spectra to our experimental traces, we processed the simulated data as follows: For each conformer, the frequencies for all the transitions given as output from MolFC (B3LYP/cc-pVDZ values) we scaled by 0.970 and shifted in order to place the band origin at the value predicted by G2 theory. Each line of the 0 K Franck–Condon spectrum was convoluted with the calculated sequence band stick profile, and a Gaussian line width of 16 cm⁻¹ (fwhm) was applied. This line width was estimated from room temperature rotational simulations using our SpecView software; rotational constants from MP2/6-31G(d) equilibrium geometries of each conformer were utilized. In order to make intensity comparisons among the conformers the simulated spectra were weighted by ab initio relative Boltzmann factors (G2) and electronic transition oscillator strengths. Throughout the remainder of this work, simulated spectra generated by this procedure are dubbed “full” simulations.

5. Results

5.1. Computational Results. On the basis of our calculations, a few general observations can be made on the observed spectra before proceeding to a detailed analysis. Table 1 lists origin frequencies for the anticipated conformers of both peroxies computed with density functional theory calculations at the B3LYP/cc-pVDZ level and with ab initio calculations using the G2 method, along with relative energies and equilibrium Boltzmann populations. Computationally, all four anticipated conformers of cyclohexyl peroxy were found to be minima on the potential energy surface in both \tilde{X} and \tilde{A} electronic states.

Due to the flatness of the ring puckering potential of the cyclopentane ring, we performed geometry searches at the B3LYP level in the \tilde{X} state from several initial structures of cyclopentyl peroxy to ensure that no conformer was overlooked. We attempted to optimize the peroxy geometries in which envelope cyclopentane is substituted in all six symmetry-unique positions (labeled a–f in Figure 2), with O₂ oriented cis with respect to the ring. Interestingly, neither of the C_s-symmetric structures in which the oxygen atoms are attached in a “top of the envelope” position (a,b in Figure 2) was found to be a minimum; the “axial cis” and “equatorial cis” geometries are saddle points, each with an imaginary frequency corresponding to ring twisting motion. Geometry searches beginning with the peroxy moiety attached in positions c–f all converged to one of the mirror images of the half-chair structure labeled C in Figure 2.

We also located two distinct gauche conformers, both of which have a half-chair arrangement of the cyclopentane ring; these are labeled G₁G₂ and G₁T₂. In our notation, the first “G” or “C” refers to the orientation of the O₂ fragment with respect to the center of the ring (alternatively speaking, the “C” conformer has $D(\text{O-O-C-H}) \approx 180^\circ$, while the “G” conformers have $D(\text{O-O-C-H}) \approx \pm 60^\circ$). For the gauche conformers the second G/T label refers to a dihedral angle of $\sim 60^\circ/\sim 180^\circ$ between the terminal oxygen atom and the front carbon atom in the half-chair structure, respectively (Figure 2). Like the cis, each gauche conformer exists as a mirror image pair. In order to understand the ring puckering potential in more detail, a geometry search for the transition state connecting the \tilde{X} state G₁T₂ and G₁G₂ conformers was performed at the B3LYP level. We located a transition state structure in which the ring adopts an envelope conformation, with the oxygen atoms attached at position a (Figure 2) in a gauche O–O–C–H arrangement. The relative electronic energies (no ZPVE cor-

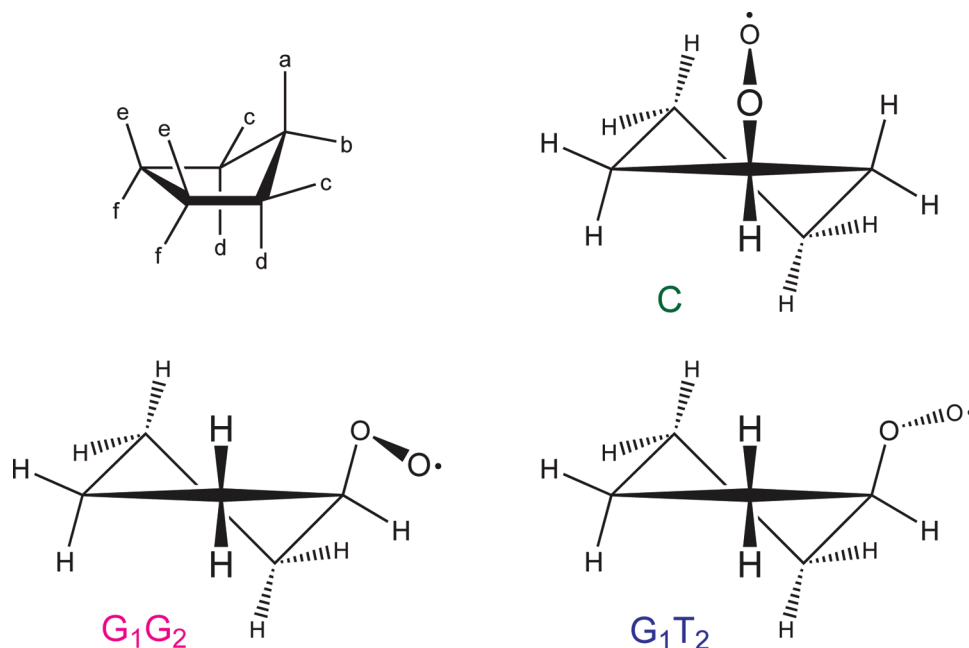


Figure 2. (Top left) Unique attachment points for the envelope conformer of cyclopentane. (Top right and bottom) Conformers of cyclopentyl peroxy. Each conformer exists as mirror image pairs.

rection) of the G_1T_2 , G_1G_2 , and transition state structures were calculated to be 0 cm^{-1} , $+151\text{ cm}^{-1}$, and $+317\text{ cm}^{-1}$, respectively.

In the \tilde{A} state, the equilibrium geometries of the two gauche conformers are very similar to their \tilde{X} state structures, while the cis-conformer adopts an envelope geometry with the O_2 group attached in position e in Figure 2. From the optimized B3LYP geometries, we performed G2 calculations in order to give more reliable relative energies. We were unable, however, to obtain a G2 energy for the \tilde{A} state of the G_1G_2 conformer. For this conformer, the first step of the G2 routine, a UHF/6-31G(d) geometry optimization, located a minimum energy structure with an envelope arrangement of the carbon atoms similar to the G_1T_2 / G_1G_2 transition state geometry found on the \tilde{X} state surface at the B3LYP level. However, the subsequent MP2/6-31G(d) geometry search beginning with this UHF envelope structure converged to the G_1T_2 \tilde{A} state geometry, not the G_1G_2 geometry as expected. Suspicious that the UHF envelope structure was a poor starting point for the MP2 search for the G_1G_2 \tilde{A} state minimum, we also initiated the MP2 geometry optimization from the B3LYP \tilde{A} state G_1G_2 equilibrium structure, and again the G_1T_2 geometry was found. We conclude that the G_1G_2 conformer has no minimum \tilde{A} state structure at the MP2 level. We do not know whether the G_1G_2 conformer would become a stable geometry if the higher order corrections were added later in the G2 routine. However, since the G_1G_2 geometry is indeed an \tilde{A} state minimum at the B3LYP level, we will provide an estimate of the origin frequency of this conformer. Taking the G2 origin of the G_1T_2 conformer and adding the difference in origin frequencies between the two gauche conformers calculated at the B3LYP level, we obtain $7460 + 7591 - 7584 = 7467\text{ cm}^{-1}$, as shown in Table 1.

From the CIS results in Table 2, we also note that the strength of the $\tilde{A}-\tilde{X}$ electronic transition exhibits a marked dependence on molecular geometry. In particular, the cis-conformers of cyclohexyl peroxy, both of which possess C_s symmetry, have oscillator strengths considerably smaller than those of the two gauche conformers. Furthermore, the oscillator strength of each equatorial conformer of cyclohexyl peroxy is about twice as

TABLE 2: Oscillator Strengths (f -values) for the $\tilde{A}-\tilde{X}$ Transitions of Cyclohexyl, Cyclopentyl, Isopropyl, and Ethyl Peroxy Radicals, As Calculated with the TD-B3LYP and CIS Methods^a

conformer	TD-B3LYP/cc-pVDZ		CIS/6-31G(d)	
	\tilde{X} geom 10^5f	\tilde{A} geom 10^5f	\tilde{X} geom 10^5f	\tilde{A} geom 10^5f
$C_6H_{11}O_2$ -eG	2.83	2.77	2.61	2.76
$C_6H_{11}O_2$ -aG	0.14	0.46	1.22	1.48
$C_6H_{11}O_2$ -eC	0.29	0.00092	0.47	0.57
$C_6H_{11}O_2$ -aC	1.81	2.72	0.24	0.15
$C_5H_9O_2$ - G_1T_2	3.21	2.33	2.24	2.29
$C_5H_9O_2$ - G_1G_2	1.52	^b	1.85	^b
$C_5H_9O_2$ -C	0.48	1.64	1.57	2.11
2- $C_3H_7O_2$ -G	1.45		2.02	
2- $C_3H_7O_2$ -T	0.71		0.26	
$C_2H_5O_2$ -G	1.02		1.92	
$C_2H_5O_2$ -T	1.40		2.09	

^a Calculations were performed using the MP2/6-31G(d) \tilde{X} state and \tilde{A} state equilibrium geometries in order to demonstrate the dependence of oscillator strengths on nuclear geometry. Results obtained using the CIS method exhibit much better agreement with experiment than those obtained using TD-B3LYP. ^b No minimum MP2/6-31G(d) \tilde{A} state geometry.

large as that of its axial counterpart. For cyclopentyl peroxy, all three conformers have C_1 symmetry and their oscillator strengths are comparable to the gauche conformers of cyclohexyl peroxy. These results are somewhat surprising since the “zeroth-order” assumption is that the oscillator strength is an electronic property, and one would expect the electronic properties of different conformers to be quite similar. The explanation may be that the $\tilde{A}-\tilde{X}$ transition is so weakly allowed, even though it is an electronic property, its strength, particularly in percentage terms, is a relatively strong function of nuclear geometry. We also found that the calculated values of the oscillator strengths depend strongly on the theoretical level used in the calculation. For example, at the TD-B3LYP/cc-pVDZ level, the aG conformer was predicted to have an f -value smaller than that of the eG by about a factor of 20. However, relative oscillator strengths calculated at the EOMEE-CCSD level are qualitatively

TABLE 3: Selected \tilde{X} and \tilde{A} State Vibrations for Conformers of Cyclohexyl and Cyclopentyl Peroxy Radicals^a

mode	\tilde{X}	\tilde{A}	description	mode	\tilde{X}	\tilde{A}	description
cyclohexyl peroxy aG				cyclohexyl peroxy eG			
ω_{51}	82	82	CO torsion	ω_{51}	84	92	CO torsion
ω_{50}	135	146	ring rock	ω_{50}	127	136	ring rock
ω_{49}	179	187	ring rock	ω_{49}	219	215	ring twist
ω_{48}	309	274	CH rock+COO bend	ω_{48}	240	221	ring rock+COO bend
ω_{47}	285	290	ring butterfly	ω_{47}	315	320	ring rock
ω_{46}	366	367	ring stretch+CH rock	ω_{46}	355	346	ring stretch
ω_{45}	411	393	ring breathe (+COO bend)	ω_{45}	426	418	ring breathe+COO bend
ω_{44}	465	468	ring breathe (no COO bend)	ω_{44}	490	445	ring breathe+COO bend
ω_{43}	524	489	ring breathe+COO bend	ω_{43}	444	452	ring butterfly (+COO bend)
ω_{40}	778	771	ring breathe+CO str+COO bend	ω_{42}	550	528	CH bend+COO bend
				ω_{36}	894	900	CO stretch+CCH bend
				ω_{35}	910	913	CCH bend+COO bend
ω_{34}	1165	966	OO stretch	ω_{34}	1148	960	OO stretch
				ω_{33}	993	994	CC stretch+CO stretch
cyclopentyl peroxy G ₁ T ₂				cyclopentyl peroxy G ₁ G ₂			
ω_{42}	57	48	ring pucker	ω_{42}	57	48	ring pucker
ω_{41}	107	142	CO torsion	ω_{41}	93	132	CO torsion
ω_{40}	218	223	ring bend+CH rock	ω_{40}	185	191	ring bend
ω_{39}	289	257	ring bend+COO bend	ω_{39}	294	268	COO bend+ring rock
ω_{38}	373	365	ring bend+COO stretch	ω_{38}	366	371	ring butterfly
ω_{37}	482	430	CH wag+COO bend	ω_{37}	502	434	COO bend+CCH bend
ω_{30}	880	888	ring breathe				
ω_{27}	1157	950	OO stretch	ω_{27}	1160	957	OO stretch
cyclohexyl peroxy eC				cyclopentyl peroxy C			
ω_{19}	1115	952	OO stretch	ω_{27}	1114	952	OO stretch
cyclohexyl peroxy- <i>d</i> ₁₁ aG				cyclohexyl peroxy- <i>d</i> ₁₁ eG			
ω_{51}	79	78	CO torsion	ω_{51}	81	87	CO torsion
ω_{50}	124	133	ring rock	ω_{50}	115	125	ring rock
ω_{49}	155	166	ring rock	ω_{49}	177	175	ring twist
ω_{48}	240	242	ring butterfly	ω_{48}	220	205	ring rock+COO bend
ω_{47}	270	249	CD rock+COO bend	ω_{47}	262	263	ring rock
ω_{46}	301	304	ring stretch+CD rock	ω_{46}	327	320	ring stretch
ω_{45}	365	343	ring breathe (+COO bend)	ω_{45}	360	360	ring butterfly (+COO bend)
ω_{44}	379	377	ring breathe (no COO bend)	ω_{44}	379	378	ring breathe+COO bend
ω_{43}	485	444	ring breathe+COO bend	ω_{43}	420	401	ring breathe+COO bend
ω_{39}	694	693	ring breathe+CO str+COO bend	ω_{42}	499	458	CD bend+COO bend
				ω_{35}	737	739	CCD bend
ω_{31}	805	806	CCD bend	ω_{32}	816	823	CO stretch+CCD bend
ω_{30}	884	883	CCD bend+CC stretch	ω_{30}	888	883	CO stretch+CCD bend
ω_{28}	919	914	CO stretch+COO bend	ω_{28}	920	918	CO stretch+CCD bend
ω_{26}	956	954	CCD bend(+OO stretch)	ω_{27}	1132	956	OO stretch+CCD bend
ω_{25}	1165	966	OO stretch	ω_{26}	1157	963	OO stretch
				ω_{25}	972	974	ring stretch+CO stretch
cyclohexyl peroxy- <i>d</i> ₁₁ eC							
ω_{16}	1170	960	OO stretch				

^a Mode numbering follows Herzberg's notation as applied to the \tilde{A} state vibrations. All vibrational frequencies (cm⁻¹) were calculated via B3LYP/cc-pVDZ and scaled ($\times 0.970$).

similar⁸² to the CIS/6-31G(d) results given in Table 2, which exhibit much better agreement with experiment.

Results of the B3LYP/cc-pVDZ harmonic vibrational frequency calculations are summarized in Table 3. Here we show the calculated frequencies used in assigning the experimental spectra; the full list is presented in Supporting Information. In order to provide a qualitative description of the active vibrations in the observed spectrum, the normal modes were animated for both the \tilde{X} and \tilde{A} state equilibrium structures. A key point is that several low frequency modes are characterized by COO bending motion coupled with displacements in the hydrocarbon ring. As COO bending modes have been observed in a variety of alkyl peroxy radicals,⁵⁴ mixing of COO bending with vibrational motion in the alkyl group plays a vital role in the vibrational structure of the $\tilde{A}-\tilde{X}$ manifolds of the cycloalkyl peroxies (vide infra).

5.2. Overview of Spectra. Figure 3 shows a survey spectrum of cyclopentyl, cyclohexyl, and cyclohexyl-*d*₁₁ peroxies over the range 6610–9260 cm⁻¹. From Table 1 we see that the intense features in the 7400–7600 cm⁻¹ region of the experimental spectrum correspond well with the computed $\tilde{A}-\tilde{X}$ band origins, particularly those from G2 theory. These values are also in the range of, but distinct from, the band origin positions of acyclic alkyl peroxy radicals reported in the literature.⁵⁴ Other intense bands, located ca. 920 cm⁻¹ to the blue of the origins, possess similar band profiles and are ascribed to O–O stretching vibrations. In the range 7600–8300 cm⁻¹ there are a series of weak-to-moderately intense features which are roughly replicated to the blue of the O–O stretch. Vibrations involving peroxy COO bending motion are expected to fall in this region with intensities similar to those observed here. Finally, several sharper features appear below 7400 cm⁻¹ for cyclopentyl and

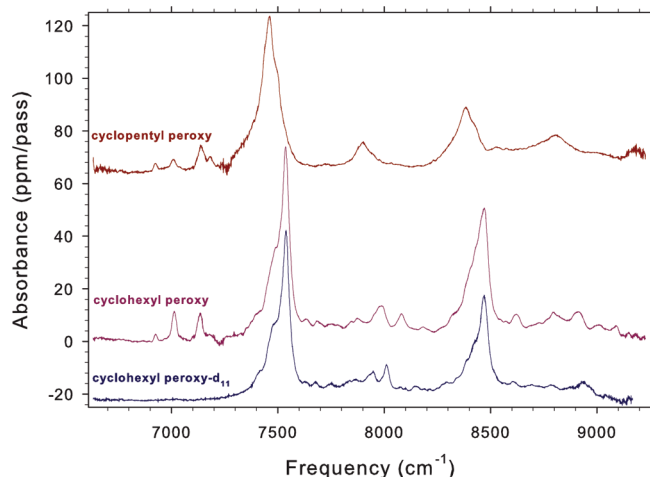


Figure 3. Survey spectra of the $\tilde{A}-\tilde{X}$ electronic transitions of cyclopentyl, cyclohexyl, and cyclohexyl- d_{11} peroxy radicals over the range 6610–9260 cm^{-1} . All traces have been digitally smoothed.

TABLE 4: Experimentally Observed Frequencies (cm^{-1}), Computed Frequencies (cm^{-1}), Franck–Condon Factors, and Assignments for Cyclopentyl Peroxy^a

band	OO str	low freq ^c	calcd	FCF	assignment
6925					^b
7006					^b
7137					^b
7180					^b
7461			7460	0.465	$G_1T_2 0_0^0$
7481		+20	+26		$G_1T_2 41 42 (?)$
			7467	0.358	$G_1G_2 0_0^0 (?)$
7495		+34	+35		$G_1T_2 41 $
7727		266	(223)	0.009	$(G_1T_2 40_0^0)$
			257	0.014	$G_1T_2 39_0^0$
			7645	0.194	$C 0_0^0 (?)$
7902		441	430	0.014	$G_1T_2 37_0^0$
			434	0.003	$G_1G_2 37_0^0$
8384	923		(888)	0.006	$(G_1T_2 30_0^0)$
			950	0.295	$G_1T_2 27_0^0$
			957	0.187	$G_1G_2 27_0^0$
8527		143	950 + 142	0.006	$G_1T_2 27_0^0 41_0^0$
			957 + 132	0.036	$G_1G_2 27_0^0 41_0^0$
			952	0.077	$C 27_0^0 (?)$
8810		427	950 + 430	0.009	$G_1T_2 27_0^0 37_0^0$

^a The calculated origin position was obtained by the G2 method; vibrational frequencies were computed at the B3LYP/cc-pVDZ level and scaled ($\times 0.970$). In cases where a single observed band is assigned to multiple transitions, minor components are given in parentheses. ^b Unknown carrier. ^c Frequency of fundamental minus origin or combination minus 0-0 stretch band.

cyclohexyl peroxies but not $C_6D_{11}O_2$. In the following paragraphs, we will consider each spectral region in turn. Measured experimental frequencies for each of the bands are given in Tables 4, 5, and 6 for cyclopentyl, cyclohexyl, and cyclohexyl- d_{11} peroxies, respectively.

6. Discussion

6.1. Bands at 6600–7400 cm^{-1} . From the calculated band origin frequencies (Table 1), the appearance of features below 7400 cm^{-1} in the spectra of Figure 3 comes as a bit of a surprise, and accordingly, we are able to rule out cyclopentyl and cyclohexyl peroxy radicals as the carriers. For cyclohexyl peroxy we found that the origin signal and the bands in this region vary in intensity independently as the gas mixture in the cell is varied, indicating that the peroxy is not the carrier. Although

the cyclohexyl peroxy aC conformer band origin is predicted here, it is unfavored on grounds of its minuscule Boltzmann weight and oscillator strength, and cyclopentyl peroxy has no conformer predicted in this region. These features are also located too far to the red of the band origins to be accounted for by hot sequence transitions from the ground state. Since the peaks are absent in the spectrum of $C_6D_{11}O_2$, they are likely overtones or combination bands of ground-state vibrations of some unknown carrier. In our “excimer off” (without photolysis) traces, we observed that cyclopentane and cyclohexane themselves possess bands which are similar, but not identical, to those in Figure 3 (see Supporting Information), while the spectrum of cyclohexane- d_{12} is silent in this region. Combination bands having two quanta of C–H stretching and one of C–C–H bending would produce the required frequencies (i.e., $2 \times 2800 + 1500 = 7100 \text{ cm}^{-1}$) in the spectra of the normal isotopomers and would be shifted well below our scanning range in the $C_6D_{11}O_2$ spectrum. (In contrast, the computed isotope shifts for the $\tilde{A}-\tilde{X}$ electronic transitions do not exceed 20 cm^{-1} (Table 1)). In the CRDS spectrum of propyl peroxy reported previously, a very similar series of bands was assigned to an unknown stable species.⁴⁴ Although we cannot assign these features to a specific carrier in the present study, in light of our experimental observations an assignment analogous to that of the propyl peroxy study seems appropriate.

6.2. Origin Region: 7400–7800 cm^{-1} . Figures 4 and 5 display the cyclopentyl and cyclohexyl peroxy band origin regions along with vibrational sequence band simulations expected for the thermally populated conformers. For cyclohexyl peroxy, sequence band simulations for conformers of the perdeuterio isotopomer are included in Supporting Information. The sequence band simulations have two limitations which should be discussed: (1) harmonic potentials are assumed for all vibrations, and (2) only sequence hot bands ($\Delta\nu = 0$) are included, while hot bands with $\Delta\nu \neq 0$ are assumed to have zero Franck–Condon factors.

The first limitation is important for the lowest frequency modes, which will have many populated vibrational levels in the \tilde{X} state (e.g., ring puckering vibrations of $C_5H_9O_2$ conformers, and C–O torsion vibrations; see Table 3). Each conformer of cyclopentyl peroxy has over a dozen puckering levels with Boltzmann factors above the threshold for inclusion in the simulations. Here, the computed barrier separating the G_1T_2 and G_1G_2 conformers in the \tilde{X} state is calculated to be only 317 cm^{-1} above the G_1T_2 minimum, yielding $317 - 151 = 166 \text{ cm}^{-1}$ above the G_1G_2 minimum. This implies that in the \tilde{X} state there will be at most only six and three bound ring puckering levels for the G_1T_2 and G_1G_2 conformers, respectively. Experimentally, transitions originating from above the barrier will “fill in” the spectrum with structureless intensity, as consistent with observation. The calculated \tilde{X} state C–O torsional potential curves⁴⁰ suggest that a similar situation is occurring for cyclohexyl peroxy. Estimated barriers for conversion between the conformers are (from DIW): aG \rightarrow aC, $\sim 1000 \text{ cm}^{-1}$; eG \rightarrow eC, $\sim 800 \text{ cm}^{-1}$; aG \rightarrow aG', $\sim 300 \text{ cm}^{-1}$; and eG \rightarrow eG', $\sim 200 \text{ cm}^{-1}$.⁴⁰ From the latter two values we expect that the experimental spectra of the gauche conformers will also be “filled in” by transitions originating from above the racemization barriers, which is again consistent with the observed spectra.

The second limitation of the simulations will lead to a misleading result if the \tilde{X} and \tilde{A} state potentials for the low frequency modes are displaced from one another enough that hot bands of the Q_1^0 -type become allowed with intensities comparable to the Q_1^1 -type sequence transitions. The experi-

TABLE 5: Experimentally Observed Frequencies (cm^{-1}), Computed Frequencies (cm^{-1}), Franck–Condon Factors, and Assignments for Cyclohexyl Peroxy ($\text{C}_6\text{H}_{11}\text{O}_2$)^a

band	OO str	low freq ^b	calcd	FCF	assignment
6924					^c
7012					^c
7135					^c
7182					^c
7420		(−50)	(−36/−19/−35)		(aG 43 [↓] /45 [↓] /48 [↓] , shoulder)
7470		0	7458	0.486	aG 0 [↓] ₀
7538		0	7547	0.472	eG 0 [↓] ₀
		(64/71)	(82)	0.033	(aG 51 [↓] ₀)
7637		99	92	0.015	eG 51 [↓] ₀
		(167)	(187)	0.007	(aG 49 [↓] ₀)
7686		148	136	0.008	eG 50 [↓] ₀
		0	7751	0.503	eC 0 [↓] ₀ (?)
7752		214	136 + 92/215	0.002/0.001	eG 50 [↓] ₀ 51 [↓] ₀ /49 [↓] ₀
		282	290/274	0.003/0.002	aG 47 [↓] ₀ /48 [↓] ₀
7843		373	393	0.010	aG 45 [↓] ₀
7871		333	320	0.003	eG 47 [↓] ₀
7988		450	(418)	0.004	(eG 45 [↓] ₀ , shoulder)
			445	0.009	eG 44 [↓] ₀
		(518)	(489)	0.006	(aG 43 [↓] ₀ , shoulder)
8083		545	528	0.006	eG 42 [↓] ₀
8184		646	528 + 92	0.001	eG 42 [↓] ₀ 51 [↓] ₀
			(445 + 221)	0.001	(eG 44 [↓] ₀ 48 [↓] ₀ , shoulder)
			(771)	0.003	(aG 40 [↓] ₀ , shoulder)
8465			966	0.275	aG 34 [↓] ₀ (shoulder)
			(900)	0.007	(eG 36 [↓] ₀)
			(913)	0.007	(eG 35 [↓] ₀)
	927		960	0.258	eG 34 [↓] ₀
			(966 + 82)	0.027	(aG 34 [↓] ₀ 51 [↓] ₀)
			(994)	0.006	(eG 33 [↓] ₀)
8618		153	960 + 92	0.017	eG 34 [↓] ₀ 51 [↓] ₀
			960 + 136	0.009	eG 34 [↓] ₀ 50 [↓] ₀
			952	0.224	eC 19 [↓] ₀ (?)
8721		256	960 + 136 + 92	0.002	eG 34 [↓] ₀ 50 [↓] ₀ 51 [↓] ₀
			(966 + 290)	0.002	(aG 34 [↓] ₀ 47 [↓] ₀)
8796			966 + 393	0.005	aG 34 [↓] ₀ 45 [↓] ₀
		331	960 + 320	0.002	eG 34 [↓] ₀ 47 [↓] ₀
8909		444	960 + 445	0.006	eG 34 [↓] ₀ 44 [↓] ₀
			(960 + 418)	0.002	(eG 34 [↓] ₀ 45 [↓] ₀)
			(966 + 489)	0.004	(aG 34 [↓] ₀ 43 [↓] ₀)
9006		541	960 + 528	0.003	eG 34 [↓] ₀ 42 [↓] ₀
9089		624	960 + 528 + 92	0.001	eG 34 [↓] ₀ 42 [↓] ₀ 51 [↓] ₀

^a The calculated origin positions were obtained by the G2 method; vibrational frequencies were computed at the B3LYP/cc-pVDZ level and scaled ($\times 0.970$). In cases where a single observed band is assigned to multiple transitions, minor components are given in parentheses. ^b Frequency of fundamental minus origin or combination minus 0-0 stretch band. ^c Unknown carrier.

mental spectra (Figure 3) exhibit weak Franck–Condon activity in the low frequency vibrations, indicating that the vibrational potentials do not shift much with electronic excitation. We conclude then that most of the hot band intensity is probably contained in $\Delta\nu = 0$ type transitions. The C conformer of cyclopentyl peroxy appears to be an exception, but assignment of any bands to this species is uncertain (vide infra).

The experimental spectrum of the gauche cyclopentyl peroxy conformers is qualitatively reproduced by the simulations, and some of the predicted sequence band structure is resolved in the experiment. The two sets of sequence bands which dominate the envelope in the simulations are the ring puckering and C–O torsion vibrations, which give rise to spacings of -9 and $+35-40 \text{ cm}^{-1}$, respectively. Ab initio calculations place the two gauche band origins less than 10 cm^{-1} apart, and although we cannot resolve their spectra, we assign the maximum at 7461 cm^{-1} in the experimental spectrum to the G_1T_2 origin since it is predicted to be the stronger transition and to lie at lower frequency. Two partially resolved features appear immediately to the blue of the 7461 cm^{-1} band, at 7481 cm^{-1} and 7495 cm^{-1} , respectively. From the simulations, the latter transition correlates

quite well with the predicted G_1T_2 41_1^{\downarrow} C–O torsion band, but no additional members of this sequence are observed. It is quite probable that, analogous to cyclohexyl peroxy, the G_1T_2 racemization barrier is reached beyond this transition. Assignment of the band at 7481 cm^{-1} is more ambiguous, as it may arise from either the $(41_1^{\downarrow} 42_1^{\downarrow})$ hot band of the G_1T_2 conformer or from the G_1G_2 origin, or perhaps from a coincidence of the two.

The cis-conformer of cyclopentyl peroxy is not readily identifiable. From Table 1 we expect that the C conformer should have an intensity roughly one-sixth that of the sum of the gauche forms if Boltzmann weights and oscillator strengths are both taken into account. Two possible candidates are the noise-level feature around 7727 cm^{-1} and the moderately intense band at 7902 cm^{-1} , both of which can also be reasonably assigned as COO bend vibrations of the G_1T_2 conformer. The 7727 cm^{-1} feature is a more favorable candidate for the C origin due to its better agreement with the G2 value, but the calculated relative intensities provide some support for assigning this conformer to the 7902 cm^{-1} band. It is also worth mentioning that the C conformer is predicted to exhibit a progression in

TABLE 6: Experimentally Observed Frequencies and Computed Frequencies (cm^{-1}) and Assignments for Cyclohexyl Peroxy- d_{11} ($\text{C}_6\text{D}_{11}\text{O}_2$)^a

band	OO str	low freq ^b	calcd	FCF	assignment
7425		(-46)	(-41/-22/-21)		(aG 43 ₁ ^ /45 ₁ ^ /47 ₁ ^ , shoulder)
7471		0	7458	0.477	aG 0 ₀ ^
7539		0	7550	0.469	eG 0 ₀ ^
		(65/71)	(78)	0.037	(aG 51 ₀ ^)
7634		95	87	0.012	eG 51 ₀ ^
		(163)	(166)	0.007	(aG 49 ₀ ^)
7679		140	125	0.009	eG 50 ₀ ^
		0	7762	0.497	eC 0 ₀ ^ (?)
7754		215	125 + 87	0.002	eG 50 ₀ ^ 51 ₀ ^
		283	304	0.006	aG 46 ₀ ^
7835		296	263	0.001	eG 47 ₀ ^
		364	343	0.007	aG 45 ₀ ^
7862		323	320	0.002	eG 46 ₀ ^
			360	0.002	eG 45 ₀ ^
7947		408	401	0.004	eG 43 ₀ ^
		(476)	(444)	0.007	(aG 43 ₀ ^)
8013		474	458	0.014	eG 42 ₀ ^
8147		608	458 + 87	0.002	eG 42 ₀ ^ 51 ₀ ^
			458 + 125	0.001	eG 42 ₀ ^ 50 ₀ ^
			401 + 205	0.001	eG 43 ₀ ^ 48 ₀ ^
		(676)	(693)	0.001	(aG 39 ₀ ^)
8293		754	739	0.003	eG 35 ₀ ^
		(822)	(806)	0.003	(aG 31 ₀ ^)
8427			(883)	0.006	(aG 30 ₀ ^)
			(914)	0.014	(aG 28 ₀ ^)
			(954)	0.007	(aG 26 ₀ ^)
	956		966	0.241	aG 25 ₀ ^
			(823)	0.005	(eG 32 ₀ ^)
			(883)	0.020	(eG 30 ₀ ^)
8467			(966 + 78)	0.026	(aG 25 ₀ ^ 51 ₀ ^)
			(918)	0.005	(eG 28 ₀ ^)
	928		963/956	0.153/0.091	eG 26 ₀ ^ /27 ₀ ^
			(974)	0.007	(eG 25 ₀ ^)
8604		137	963/956 + 87	0.009/0.005	eG 26 ₀ ^ 51 ₀ ^ /27 ₀ ^ 51 ₀ ^
			963/956 + 125	0.007/0.004	eG 26 ₀ ^ 50 ₀ ^ /27 ₀ ^ 50 ₀ ^
			(966 + 166)	0.002	(aG 25 ₀ ^ 49 ₀ ^)
			960	0.212	eC 16 ₀ ^ (?)
8693		226	963/956 + 125 + 87	0.001/0.001	eG 26 ₀ ^ 50 ₀ ^ 51 ₀ ^ /27 ₀ ^ 50 ₀ ^ 51 ₀ ^
			(963/956 + 263)	0.001/0.0004	(eG 26 ₀ ^ 47 ₀ ^ /27 ₀ ^ 47 ₀ ^)
			(966 + 304)	0.003	(aG 25 ₀ ^ 46 ₀ ^)
8782		355	966 + 343	0.004	aG 25 ₀ ^ 45 ₀ ^
			(963/956 + 320)	0.001/0.001	(eG 26 ₀ ^ 46 ₀ ^ /27 ₀ ^ 46 ₀ ^)
8882			963/956 + 401	0.002/0.001	eG 26 ₀ ^ 43 ₀ ^ /27 ₀ ^ 43 ₀ ^
		415	966 + 444	0.004	aG 25 ₀ ^ 43 ₀ ^
8935		468	963/956 + 458	0.004/0.003	eG 26 ₀ ^ 42 ₀ ^ /27 ₀ ^ 42 ₀ ^
9041		574	963/956 + 458 + 87	0.001/0.0005	eG 26 ₀ ^ 42 ₀ ^ 51 ₀ ^ /27 ₀ ^ 42 ₀ ^ 51 ₀ ^

^a The calculated origin positions were obtained by the G2 method; vibrational frequencies and isotope shifts were computed at the B3LYP/cc-pVDZ and scaled ($\times 0.970$). In cases where a single observed band is assigned to multiple transitions, minor components are given in parentheses. ^b Frequency of fundamental minus origin or combination minus 0-0 stretch band.

the lowest frequency mode, corresponding to the change of ring geometry in the \tilde{A} state. The shape of the “full” cis-simulated spectrum (Figure 8) bears some resemblance to the bands at 7902 and 8810 cm^{-1} . Other possibilities are that the C conformer origin may too weak to be observed, or that it may be masked by the blue tail of the G_1T_2/G_1G_2 origin. We will consider further the location of the C origin in Section 6.4.

Cyclohexyl peroxy possesses an origin region spectrum which appears as a trimodal contour, with band maxima that compare favorably with G2-computed T_{00} values for the aG and eG conformers (Table 1). We therefore assign the shoulder at 7470 cm^{-1} and the peak pair at 7538 cm^{-1} to the predicted aG and eG conformer origins, respectively. Contours obtained from the sequence band simulations also support this assignment, giving a very reasonable example of two similar peroxy conformers which can be distinguished on the basis of hot band structure.

As manifested by the simulations, the C–O torsion frequency of the aG conformer is the same in both electronic states and does not contribute to broadening the envelope. Structure on the blue side of the aG origin arises from sequences in ω_{49} and ω_{50} , while the distinct shoulder on the red at ca. 7420 cm^{-1} is due to sequences in three nearly coincident vibrations, ω_{43} , ω_{45} , and ω_{48} . In the case of the eG conformer, the lowest sets of sequence bands, in ω_{51} (C–O torsion) and ω_{50} (ring bend), yield the majority of the structure to the blue of the origin, while the next two lowest modes, ω_{49} and ω_{48} , produce most of the structure to the red. For the eG conformer, the leftmost of the two strongest bands in the simulation corresponds to the origin, not the slightly more intense feature on the right which is a coincidence of several hot bands. Experimentally, both features are resolved.

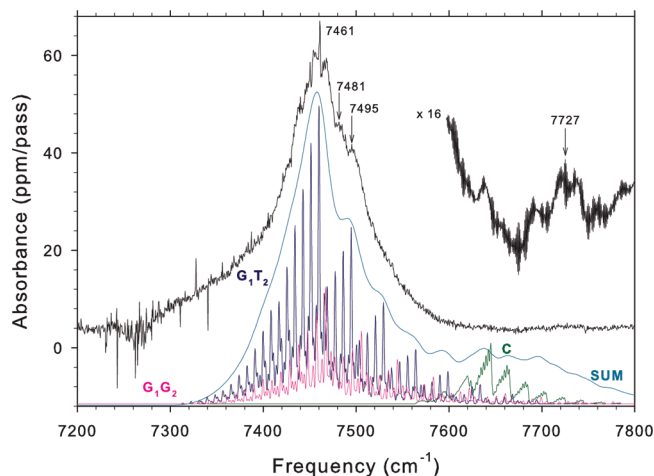


Figure 4. Origin region of cyclopentyl peroxy radical: experimental spectrum (top trace) and 298 K sequence band simulations for the three conformers (below). A line width of 2 cm^{-1} was applied to the simulations in order to emphasize the large number of transitions contained in the envelopes. Sequence band profiles have been weighted by calculated Boltzmann factors and oscillator strengths. The “full” simulation (broad trace) is shown for comparison. Simulated intensities have been scaled in order to render the strongest band (the G_1T_2 band origin) comparable to the corresponding experimental feature.

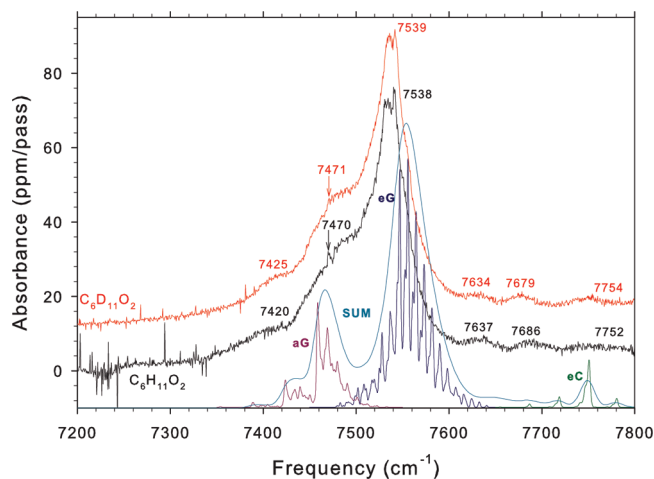


Figure 5. Origin region of cyclohexyl and cyclohexyl- d_{11} peroxy radicals: experimental spectra (top traces), and 298 K sequence band simulations for the three conformers predicted to have the greatest intensity. Narrow line (2 cm^{-1} fwhm) simulations highlight the complexity of the sequence band structure. Sequence band profiles have been weighted by calculated Boltzmann factors and oscillator strengths. The “full” simulation (broad trace) is shown for comparison. Simulated intensities have been scaled in order to render the strongest band (the eG band origin) comparable to the corresponding experimental feature.

Analogous to the C conformer of cyclopentyl peroxy, we cannot easily identify the eC origin. Although the calculated Boltzmann factor of the eC form is less than the eG by only a factor of 3, the $\tilde{A}-\tilde{X}$ electronic transition of the eC conformer is disfavored (relative to the gauche forms) by its significantly smaller oscillator strength. Since the latter quantity is difficult to calculate accurately, this conformer may be even weaker than predicted. We do expect that the eC origin is responsible, at least in part, for one of the weak features in the $7600\text{--}7900\text{ cm}^{-1}$ region. However, the numerous weak bands present are also mostly well-accounted for by Franck–Condon active vibrations of the aG and eG conformers (Figures 6 and 7). We will discuss a plausible assignment for the eC origin upon consideration of the O–O stretch region (Section 6.4).

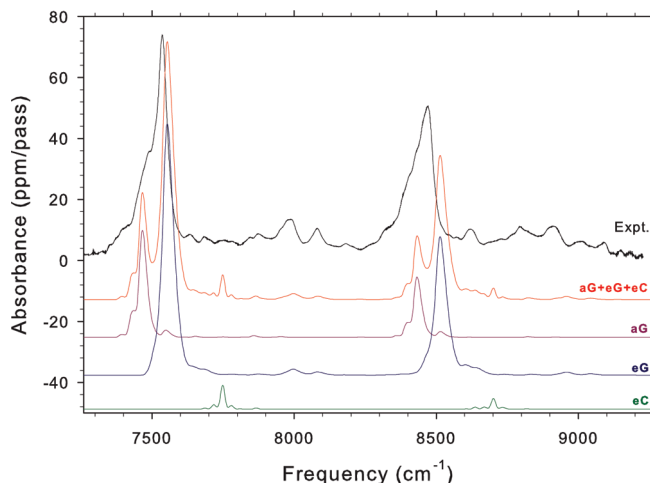


Figure 6. Experimental spectrum of cyclohexyl peroxy, along with “full” simulations of the eC, eG, and aG conformers. The experimental trace has been digitally smoothed. Simulated intensities have been scaled in order to render the strongest band (the eG band origin) comparable to the corresponding experimental feature.

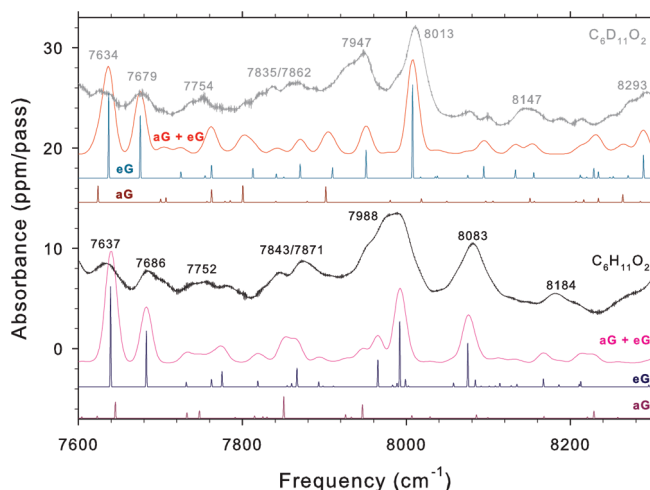


Figure 7. Experimental spectra of the COO bend regions for cyclohexyl and cyclohexyl- d_{11} peroxy radicals along with 0 K Franck–Condon simulations of the gauche conformers. Narrow line width simulations demonstrate correspondence between observed bands and computed transitions; broad simulations are presented to show overall agreement. Simulated intensities have been scaled in order to render the strongest COO bend band for each isotopomer comparable to the corresponding experimental feature. Relative to Figure 6, the y-axes of the simulated traces have been expanded by greater proportions than that of the experimental traces. Both experimental traces have been digitally smoothed.

As a side note, the previous assignment of the T (C_s symmetric) conformer of isopropyl peroxy had some ambiguity due to its low intensity and large shift from the G2 calculated frequency.⁴⁵ Oscillator strengths calculated at the CIS/6-31G(d) level for the T and G conformers of isopropyl peroxy show a similar trend to those of the conformers of cyclohexyl peroxy: the isopropyl peroxy T conformer has a much lower oscillator strength than the G conformer (Table 2). In contrast, at the same level of theory the T conformer of ethyl peroxy (C_s symmetry) has a slightly *larger* oscillator strength than the G conformer (C_1 symmetry). It appears that a key factor is the orientation of the O_2 moiety with respect to the alkyl groups; that is, a gauche R–C–O–O arrangement (R = alkyl) results in a lower oscillator strength than a *trans*-R–C–O–O arrangement. Thus the T conformer of ethyl peroxy has a comparable, but slightly

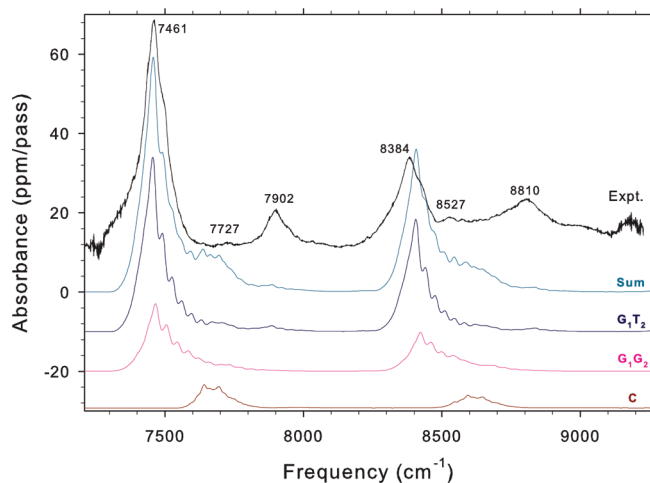


Figure 8. Experimental spectrum of cyclopentyl peroxy, along with “full” simulations of the three conformers. The experimental trace has been digitally smoothed. Simulated intensities have been scaled in order to render the strongest band (the G_1T_2 band origin) comparable to the corresponding experimental feature.

larger oscillator strength than the G conformer. For isopropyl peroxy the T conformer has O_2 doubly gauche to the alkyl groups, while the G conformer has only a single gauche arrangement, and accordingly, the T conformer is weaker. Extending this argument to cyclopentyl and cyclohexyl peroxies, the weak “cis” conformers have doubly gauche R–C–O–O structures, while the stronger “gauche” conformers have only one gauche R–C–O–O arrangement.

As a final note, the spectrum of $C_6D_{11}O_2$ is qualitatively very similar to that of $C_6H_{11}O_2$ in this region. This result is consistent with the small isotope shifts predicted by the calculations for the $\tilde{A}-\tilde{X}$ origins of all the conformers.

6.3. Bands at 7600–8300 cm^{-1} . In the 7600–8300 cm^{-1} portion of the spectrum we expect to observe the COO bending bands. One feature relevant to assigning the spectra of both peroxies is that COO bending motion is spread over several vibrations with frequencies in the range 200–600 cm^{-1} (Table 3); this is also the case for *tert*-butyl and neopentyl peroxies, which have two to three observable COO bending frequencies at 230–480 cm^{-1} above the band origin.⁴⁸ As shown in Figures 6 and 8, the *computed* relative Franck–Condon factors for COO bend vibrations (as compared to the band origins) are considerably smaller than in the experiment, while those for the O–O stretch bands are in good agreement. As discussed in section 5.1, if the electronic transition moment is a relatively strong function of nuclear position, it may be that bending the COO moiety increases the oscillator strength, resulting in COO bending bands that are stronger experimentally than expected from the FCFs. In Table 2 we see that the CIS/6-31G(d) oscillator strengths for the $\tilde{A}-\tilde{X}$ transitions are 5–30% higher for the \tilde{A} state equilibrium geometries than for the \tilde{X} state equilibrium structures for most of the conformers, suggesting that displacement in some of the active vibrational modes increases the magnitude of the electronic transition moment.

In the spectrum of cyclopentyl peroxy (Figure 8), the simulation predicts two active COO bending vibrations for the G_1T_2 conformer near the observed features at 7727 and 7902 cm^{-1} . In Table 4 both features have been assigned to these vibrations, and the lower frequency band as a possible candidate for the C origin. Since the G2 method has proven to be quite reliable in predicting peroxy $\tilde{A}-\tilde{X}$ transition frequencies, we prefer to assign the 7902 cm^{-1} band as a G_1T_2 COO bend rather than to the C origin.

A proliferation of weak bands are observable in the spectrum of cyclohexyl peroxy, most of which display one-to-one correspondence with similar bands in the cyclohexyl peroxy- d_{11} spectrum. Under the expectation that multiple COO bending modes might be active for both conformers, Franck–Condon simulations were particularly illustrative, as shown in Figure 7. Assignments are given in Tables 5 and 6. Several ring bending vibrations are active, along with the low frequency C–O torsion mode. For the aG conformer, the torsional band is not resolved as it overlaps the eG origin. Coincidence of the eG C–O torsion and a ring rocking mode of the aG gives rise to the bump at 7637 cm^{-1} , and the ring rocking vibration of the eG correlates favorably with the feature at 7686 cm^{-1} . Corresponding bands in the $C_6D_{11}O_2$ spectrum are assigned similarly. At 7752 cm^{-1} is a broad, weak feature which appears to be slightly more localized in the deuterated spectrum; in both spectra this feature results from several feeble coinciding bands of the two gauche conformers.

In the range 7800–8200 cm^{-1} the most intense COO bending vibrations are found. The first band, at 7843/7871 cm^{-1} , has a bimodal shape, suggesting overlap of multiple features. An aG COO bend computed at 393 cm^{-1} above the origin and a weak eG ring distortion mode 320 cm^{-1} above its origin roughly correspond to this feature. The next two bands, at 7988 and 8083 cm^{-1} , are remarkably well-reproduced by the simulation, as are the two eG COO bending modes which carry the majority of the Franck–Condon activity. The lower frequency band is more intense in the spectrum of $C_6H_{11}O_2$, with one of the aG COO bending vibrations adding intensity to the red shoulder of the 7988 cm^{-1} band, which already includes two moderately strong eG transitions. In the $C_6D_{11}O_2$ spectrum, the feature at 8013 cm^{-1} corresponds to the most intense COO bend band of the eG conformer, at 458 cm^{-1} above the origin. Beyond the highest-frequency COO bend, the spectrum is more difficult to assign. Between 8083 cm^{-1} and 8400 cm^{-1} , we expect to observe a myriad of ring displacement modes and COO bend/C–O torsion combination bands, all of which have feeble Franck–Condon activity. The peak at 8184 cm^{-1} in the $C_6H_{11}O_2$ spectrum appears to be a synchronous set of peaks from both conformers, while the deuterated spectrum has these transitions spread out over several small maxima. For this reason, the maxima at 8184 cm^{-1} ($C_6H_{11}O_2$) and 8147 cm^{-1} ($C_6D_{11}O_2$) are not clearly assignable to a few transitions, but we have listed the main contributors, on the basis of simulations, in Tables 5 and 6. Finally, at 8293 cm^{-1} in the $C_6D_{11}O_2$ spectrum we find a coincidence of two CCD bending bands, one from each of the gauche conformers.

6.4. Bands at 8300–9260 cm^{-1} . Above 8300 cm^{-1} the spectrum of cyclopentyl peroxy is expressed as only three bands. The O–O stretch vibrations of the G_1T_2 / G_1G_2 conformers are easily assigned to the large feature at 8384 cm^{-1} , while the spacing between this peak and that at 8810 cm^{-1} is consistent with an O–O stretch/COO bend combination band. At 8527 cm^{-1} is a faint feature which lies 143 cm^{-1} beyond the gauche O–O stretch, in excellent agreement with either of the gauche conformer C–O torsion frequencies. In the simulations the Franck–Condon factors for the torsion bands are larger in the origin region than in the O–O stretch region. However, in the experimental spectrum the torsion bands predicted in the origin region fall within the broad envelope of the band origin and are not resolved. It is therefore worth considering whether the band at 8527 cm^{-1} could also be reasonably assigned to the C conformer O–O stretch, which would similarly place the C *origin* inside the broad envelope in the range 7400–7600 cm^{-1} .

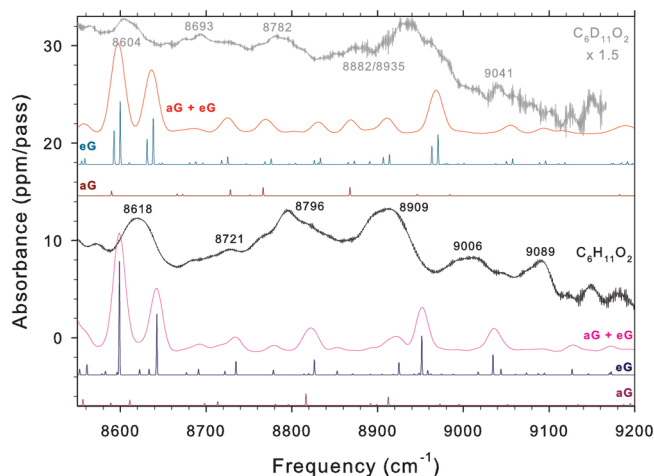


Figure 9. Experimental spectra of the OO stretch regions for cyclohexyl and cyclohexyl- d_{11} peroxy radicals along with 0 K Franck–Condon simulations. Narrow line width simulations demonstrate correspondence between observed bands and computed transitions; broad simulations are presented for overall agreement. Simulated intensities have been scaled in order to render the strongest band for each isotopomer comparable to the corresponding experimental feature. Relative to Figure 6, the y-axes of the simulated traces have been expanded by greater proportions than that of the experimental traces. Both experimental traces have been digitally smoothed.

Redshifting the O–O stretch to 8527 cm^{-1} , we deduce an origin frequency of $8527 - 952 = 7575\text{ cm}^{-1}$ for the C conformer. Here, the C origin may go unresolved in the envelope of the more intense gauche spectra. This deduced value of the C origin differs from the G2 prediction by 70 cm^{-1} . If this assignment is correct, the agreement with G2 is not as good as that for the $G1T_2$ origin, but 7575 cm^{-1} is closer to the G2 value for the C origin than either of the 7727 cm^{-1} or 7902 cm^{-1} bands. While this assignment is not definitive, we find it attractive in light of similar arguments for cyclohexyl peroxy (vide infra).

From $8300\text{--}9260\text{ cm}^{-1}$ the spectrum of cyclohexyl peroxy for the most part resembles that below 8300 cm^{-1} . The O–O stretch feature, consisting of a superposition of the aG and eG transitions, reaches a maximum at 8465 cm^{-1} . A number of weaker bands with moderate Franck–Condon activity are also buried in the O–O stretch envelope, hence the large number of transitions listed in Tables 5 and 6. In the spectrum of $C_6D_{11}O_2$ we can distinguish the O–O stretch peaks of both conformers, but the eG conformer actually possess two O–O stretching vibrations with substantial Franck–Condon activity, ω_{26} and ω_{27} . The O–O stretches of the two conformers differ by $\sim 40\text{ cm}^{-1}$, which facilitates assignment of the O–O stretch/COO bend combination bands. Figure 9 shows an expansion of the weak features to the blue of the O–O stretch region. From the Franck–Condon factors in Table 5 we see that the lowest frequency vibrations of the eG conformer have greater intensity in combination with the O–O stretch than they do in the origin region. This is evidently a result of mode mixing with the O–O stretch and results in higher intensity than expected for the combination band at 8618 cm^{-1} , which is apparently a coincidence of two separate features.

However, an alternative explanation for the large intensity of the band at 8618 cm^{-1} is to assign it, at least in part, to the eC O–O stretch, by analogy with the 8527 cm^{-1} band of cyclopentyl peroxy. For the eG conformer the simulation shows two resolved weak bands, both near the origin (Figure 7) and near the O–O stretch (Figure 9). In the origin region the eG 51_0^1 and 50_0^1 bands at 7637 cm^{-1} and 7686 cm^{-1} are predicted

to appear with the higher frequency band weaker in intensity by a factor of 2. Experimentally, the intensities of the two bands are nearly equal, which leads us to consider a possible additional carrier for the 7686 cm^{-1} band. In the O–O stretch region, we expect two resolved eG combination bands, namely $34_0^1 51_0^1$ and $34_0^1 50_0^1$, but these are *not* resolved experimentally. In Figure 6 the O–O stretch band in the simulated spectrum of the eC conformer compares favorably with the feature at 8618 cm^{-1} if the simulation of the eC conformer is red-shifted by $\sim 80\text{ cm}^{-1}$. Placing the O–O stretch of the eC conformer at 8618 cm^{-1} would result in a single broad feature in which the eC O–O stretch is coincident with two nearby eG features. The eC band origin would therefore appear at $8618 - 952 = 7666\text{ cm}^{-1}$, in good agreement with the feature at 7686 cm^{-1} . This would also explain the similarities in intensity observed for the 7637 cm^{-1} and 7686 cm^{-1} bands. Comparison of the G2 value for the eC origin with the experimental feature at 7686 cm^{-1} is also reasonable; the deviation $\text{expt} - G2 = -65\text{ cm}^{-1}$ here is similar to that calculated for the C origin of cyclopentyl peroxy (-70 cm^{-1}) using similar logic. As in the case of cyclopentyl peroxy, this assignment cannot be made with certainty, but it has the strength of giving a consistent analysis of the spectra of both peroxies.

The next feature of the cyclohexyl peroxy spectrum, a faintly distinguishable shoulder at 8721 cm^{-1} , we assign analogously to the band at 7752 cm^{-1} : several weak bands from both conformers with the addition of a quantum of O–O stretching. At 8796 and 8909 cm^{-1} are two rather strong bands; these are separated from the O–O stretch band by typical COO bending frequencies, similar to the bands at ca. 8000 cm^{-1} . The simulation suggests that the 8796 cm^{-1} feature results from transitions from two different conformers. This band lies 925 cm^{-1} above the feature at 7871 cm^{-1} and 953 cm^{-1} above that at 7843 cm^{-1} . An O–O stretch of 953 cm^{-1} is similar to that of the deuterated aG conformer, allowing us a cross-check for the assignment of the 7843 cm^{-1} band to the aG COO bend. Additionally, the spacing of 925 cm^{-1} is consistent with an eG O–O stretch, which provides more confidence that our assignment of 7871 cm^{-1} to an eG vibration is correct. The best equatorial gauche match for the 7871 cm^{-1} band indeed appears to be the ring rock vibration with a frequency of 320 cm^{-1} . Returning to the combination band region, the feature at 8909 cm^{-1} appears to have several contributing transitions, the strongest of which involves the eG COO bend at 444 cm^{-1} in combination with the O–O stretch. The band maximum is above the feature at 7988 cm^{-1} by 921 cm^{-1} , characteristic of an eG O–O stretch. Similarly, at 9006 cm^{-1} we find a feature which is 922 cm^{-1} above that at 8083 cm^{-1} and correlates well with the eG COO bend computed at 528 cm^{-1} . The last feature, at 9089 cm^{-1} , is most likely composed of several transitions from both conformers; we have assigned it in Table 5 based on the strongest nearby transition in the simulation, an O–O stretch/COO bend/C–O torsion combination. The intensities of the various bands which comprise this peak likely change when in combination with an O–O stretch; hence, the band maximum appears only 905 cm^{-1} above the 8184 cm^{-1} peak, not at an exact O–O stretch frequency for either of the conformers. Finally, assignment of the spectrum of $C_6D_{11}O_2$ follows from that of $C_6H_{11}O_2$ fairly straightforwardly. Most of the combination bands in the cyclohexyl peroxy- h_3 spectrum are reproduced in the deuterated spectrum with isotope shifts of a few wavenumbers.

7. Conclusion

In this work, we report the $\tilde{A}-\tilde{X}$ absorption spectra of cyclopentyl, cyclohexyl, and cyclohexyl- d_{11} peroxy radicals, as measured by ambient temperature cavity ringdown spectroscopy. For all three species, the spectra obtained are consistent with calculated predictions for the gauche conformers, while calculations do not permit any band to be uniquely assignable to a cis-conformer of either peroxy, although plausible assignments are discussed. Although some of the cis-conformers would be expected to be observable on the basis of their Boltzmann populations, overlap of their band origins with vibrational features of the gauche forms and smaller oscillator strengths are viable explanations for the ambiguity of their assignments or lack of observation. The spectrum of cyclopentyl peroxy is well explained by a pair of coinciding gauche conformers, perhaps with contributions from the C conformer in the COO bend region. The spectrum of cyclohexyl peroxy is most clearly interpreted as the superposition of two gauche conformers, with axial and equatorial ring substitution, respectively. Shapes of the electronic origin bands are well reproduced by hot band simulations, and Franck-Condon simulations provide evidence for numerous active COO bend vibrations, particularly in the case of cyclohexyl peroxy.

Acknowledgment. We acknowledge the financial support of this work by the DOE via Grant DE-FG02-01ER14172 and a grant of computer time from the Ohio Supercomputer Center. We gratefully acknowledge Prof. John F. Stanton (University of Texas) for useful discussion and independent Franck-Condon factor and transition dipole moment calculations. We gratefully acknowledge Dr. Raffaele Borrelli (University of Salerno) for providing technical assistance regarding the MolFC package.

Supporting Information Available: (1) experimental spectrum of $C_6H_{11}O_2$ and $C_6D_{11}O_2$ in comparison with hot band simulations for $C_6D_{11}O_2$ conformers. (2) experimental spectra of $C_6H_{11}O_2$ and $C_6H_9O_2$ in comparison with spectra of cyclohexane and cyclopentane. (3) unscaled vibrational frequencies for cyclopentyl peroxy conformers. (4) unscaled vibrational frequencies for cyclohexyl peroxy conformers. (5) energies and Cartesian coordinates of optimized geometries. This information is available free of charge via the Internet at <http://pubs.acs.org>.

References and Notes

- Wang, S.; Miller, D. L.; Cernansky, N. P.; Curran, H. J.; Pitz, W. J.; Westbrook, C. K. *Combust. Flame* **1999**, *118*, 415.
- Curran, H. J.; Gaffuri, P.; Pitz, W. J.; Westbrook, C. K. *Combust. Flame* **1998**, *114*, 149.
- Pilling, M. J.; Smith, I. W. M. In *Modern Gas Kinetics: Theory, Experiment, and Application*; Blackwell Scientific Publications: Oxford, 1987; Chap. C1-C2.
- Robertson, S. H.; Seakins, P. W.; Pilling, M. J. In *Low-temperature combustion and autoignition*; Elsevier: Amsterdam, 1997; Chap. 2.
- D'Anna, A.; Violi, A.; D'Alessio, A. *Combust. Flame* **2000**, *121*, 418.
- Zhao, F.; Asmus, T. W.; Assanis, D. N.; Dec, J. E.; Eng, J. A.; Najt, P. M. *Homogeneous Charge Compression Ignition (HCCI) Engines: Key Research and Development Issues*; Society of Automotive Engineers: Pittsburgh, PA, 2003.
- Farrell, J. T.; Cernansky, N. P.; Dryer, F. L.; Friend, D. G.; Hergart, C. A.; Law, C. K.; McDavid, R. M.; Mueller, C. J.; Patel, A. K.; Pitsch, H. *SAE Tech. Pap. Ser.* **2007**, *201*, 1.
- Pitz, W. J.; Cernansky, N. P.; Dryer, F. L.; Egolfopoulos, F. N.; Farrell, J. T.; Friend, D. G.; Pitsch, H. *SAE Tech. Pap. Ser.* **2007**, *175*, 1.
- Simon, V.; Simon, Y.; Scacchi, G.; Baronnet, F. *Can. J. Chem.* **1997**, *75*, 575.
- Crawford, M. A.; Szente, J. J.; Maricq, M. M.; Francisco, J. S. *J. Phys. Chem. A* **1997**, *101*, 5337.
- DeSain, J. D.; Taatjes, C. A. *J. Phys. Chem. A* **2001**, *105*, 6646.
- Eberhard, J.; Howard, C. J. *J. Phys. Chem. A* **1997**, *101*, 3360.
- Rowley, D. M.; Lesclaux, R.; Lightfoot, P. D.; Noziere, B.; Wallington, T. J.; Hurley, M. D. *J. Phys. Chem.* **1992**, *96*, 4889.
- Rowley, D. M.; Lightfoot, P. D.; Lesclaux, R.; Wallington, T. J. *J. Chem. Soc., Faraday Trans.* **1992**, *88*, 1369.
- Sirjean, B.; Buda, F.; Hakka, H.; Fournet, R.; Warth, V.; Battin-Leclerc, F.; Ruiz-Lopez, M. *Proc. Combust. Inst.* **2007**, *31*, 277.
- McCarthy, R. L.; MacLachlan, A. *J. Chem. Phys.* **1961**, *35*, 1625.
- James, H. W. S.; Currie, L.; Tedder, J. M. *J. Chem. Soc., Faraday Trans. 1* **1974**, *70*, 1851.
- Handford-Styring, S. M.; Walker, R. W. *Phys. Chem. Chem. Phys.* **2001**, *3*, 2043.
- Platz, J.; Sehested, J.; Nielsen, O. J.; Wallington, T. J. *J. Phys. Chem. A* **1999**, *103*, 2688.
- Rowley, D. M.; Lightfoot, P. D.; Lesclaux, R.; Wallington, T. J. *J. Chem. Soc., Faraday Trans.* **1991**, *87*, 3221.
- Gulati, S. K.; Walker, R. W. *J. Chem. Soc., Faraday Trans. 2* **1989**, *85*, 1799.
- LeMaire, M. C. O.; Ribaucour, M.; Minetti, R. *Combust. Flame* **2001**, *127*, 1971.
- Hanson, B. N. D.; Orlando, J.; Kosciuch, E. *Int. J. Mass. Spectrom.* **2004**, *239*, 147.
- Knepp, A. M.; Meloni, G.; Jusinski, L. E.; Taatjes, C. A.; Cavallotti, C.; Klippenstein, S. J. *Phys. Chem. Chem. Phys.* **2007**, *9*, 4315.
- Ive Hermans, J. P.; Jacobs, P. A. *J. Phys. Chem. A* **2008**, *112*, 1747.
- Fernandes, R. X.; Zádor, J.; Jusinski, L. E.; Miller, J. A.; Taatjes, C. A. *Phys. Chem. Chem. Phys.* **2009**, *11*, 1320.
- Law, M. E. Ph.D. thesis, University of Massachusetts-Amherst, 2005.
- Buda, F.; Heyberger, B.; Fournet, R.; Glaude, P.-A.; Warth, V.; Battin-Leclerc, F. *Energy Fuels* **2006**, *20*, 1450.
- Zhang, H. R.; Huynh, L. K.; Kungwan, N.; Yang, Z.; Zhang, S. *J. Phys. Chem. A* **2007**, *111*, 4102.
- Simmie, J. M. *Prog. Energy Combust. Sci.* **2003**, *29*, 599.
- Ranzi, E.; Dente, M.; Goldaniga, A.; Bozzano, G.; Faravelli, T. *Prog. Energy Combust. Sci.* **2001**, *27*, 99.
- Silke, E. J.; Pitz, W. J.; Westbrook, C. K.; Ribaucour, M. *J. Phys. Chem. A* **2007**, *111*, 3761. 2007.
- Granata, S.; Faravelli, T.; Ranzi, E. *Combust. Flame* **2003**, *132*, 533.
- Lightfoot, P. D.; Cox, R. A.; Crowley, J. N.; Destriau, M.; Hayman, G. D.; Jenkin, M. E.; Moortgat, G. K.; Zabel, F. *Atmos. Environ.* **1992**, *26A*, 1805.
- Wallington, T. J.; Dagaut, P.; Kurylo, M. J. *Chem. Rev.* **1992**, *92*, 667.
- Frost, G. J.; Ellison, G. B.; Vaida, V. *J. Phys. Chem. A* **1999**, *103*, 10169.
- Nielsen, O. J.; Wallington, T. J. *Ultraviolet Absorption Spectra of Peroxy Radicals in the Gas Phase in Peroxyl Radicals*; John Wiley and Sons: New York, 1997; p 69.
- Hayon, E.; Simic, M. *J. Phys. Chem.* **1971**, *75*, 1677.
- Bennett, J. E.; Summers, R. *Trans. Faraday Soc.* **1973**, *69*, 1043.
- DiLabio, G. A.; Ingold, K. U.; Walton, J. C. *J. Org. Chem.* **2007**, *72*, 8095.
- Weisman, J. L.; Head-Gordon, M. *J. Am. Chem. Soc.* **2001**, *123*, 11686.
- Jafri, J. A.; Phillips, D. H. *J. Am. Chem. Soc.* **1990**, *112*, 2586.
- Pushkarsky, M. B.; Zalyubovsky, S. J.; Miller, T. A. *J. Chem. Phys.* **2000**, *112*, 10695.
- Zalyubovsky, S. J.; Glover, B. G.; Miller, T. A.; Hayes, C.; Merle, J. K.; Hadad, C. M. *J. Phys. Chem. A* **2005**, *109*, 1308.
- Tarczay, G.; Zalyubovsky, S. J.; Miller, T. A. *Chem. Phys. Lett.* **2005**, *406*, 81.
- Glover, B. G.; Miller, T. A. *J. Phys. Chem. A* **2005**, *109*, 11191.
- Rupper, P.; Sharp, E. N.; Tarczay, G.; Miller, T. A. *J. Phys. Chem. A* **2007**, *111*, 832.
- Sharp, E. N.; Rupper, P.; Miller, T. A. *J. Phys. Chem. A* **2008**, *112*, 1445.
- Newman, S. M.; Lane, I. C.; Orr-Ewing, A. J.; Newnham, D. A.; Ballard, J. J. *Chem. Phys.* **1999**, *110*, 10749.
- Miller, T. A. *Mol. Phys.* **2006**, *104*, 2581.
- Just, G. M. P.; McCoy, A. B.; Miller, T. A. *J. Chem. Phys.* **2007**, *127*, 044310.
- Zalyubovsky, S. J.; Glover, B. G.; Miller, T. A. *J. Phys. Chem. A* **2003**, *107*, 7704.
- Just, G. M. P.; Sharp, E. N.; Zalyubovsky, S. J.; Miller, T. A. *Chem. Phys. Lett.* **2006**, *417*, 378.
- Sharp, E. N.; Rupper, P.; Miller, T. A. *Phys. Chem. Chem. Phys.* **2008**, *10*, 3955.
- Chung, C.-Y.; Cheng, C.-W.; Lee, Y.-P.; Liao, H.-Y.; Sharp, E. N.; Rupper, P.; Miller, T. A. *J. Chem. Phys.* **2007**, *127*, 044311.
- Dixon, D.; Komornicki, A. *J. Phys. Chem.* **1990**, *94*, 5630.
- Kilpatrick, J. E.; Pitzer, K. S.; Spitzer, R. *Chem. Rev.* **1947**, *69*, 2483.

- (58) Kilpatrick, J. E.; Pitzer, K. S.; Spitzer, R. *Chem. Rev.* **1947**, 69, 2483.
- (59) Tomimoto, M.; Go, N. *J. Chem. Phys.* **1995**, 99, 563.
- (60) Durig, J. R.; Wertz, D. W. *J. Chem. Phys.* **1968**, 49, 2118.
- (61) Bauman, L. E.; Laane, J. *J. Phys. Chem.* **1988**, 92, 1040.
- (62) Sax, A. F. *Chem. Phys.* **2008**, 349, 9.
- (63) Hilderbrandt, R. L.; Shen, Q. *J. Phys. Chem.* **1982**, 86, 587.
- (64) Groner, P.; Lee, M. J.; Durig, J. R. *J. Chem. Phys.* **1991**, 94, 3315.
- (65) Durig, J. R.; Zhao, W.; Zhu, X. *J. Mol. Struct.* **2000**, 521, 25.
- (66) Badawi, H. M.; Herrebout, W. A.; Mohamed, T.; der Veken, B. V.; Sullivan, J. F.; Durig, D. T.; Zheng, C.; Kalasinsky, K. S.; Durig, J. R. *J. Mol. Struct.* **2003**, 645, 89.
- (67) Bickford, C.; Shen, Q. *J. Mol. Struct.* **2001**, 567/568, 269.
- (68) Hilderbrandt, R. L.; Leavitt, H.; Shen, Q. *J. Mol. Struct.* **1984**, 116, 29.
- (69) Choe, J.-I.; Harmony, M. D. *J. Mol. Spectrosc.* **1980**, 81, 480.
- (70) Nandi, R. N.; Harmony, M. D. *J. Mol. Spectrosc.* **1983**, 98, 221.
- (71) Durig, J. R.; Zhao, W.; Zhu, X.; Geyer, T. J.; Dakkouri, M. *J. Mol. Struct.* **1995**, 351, 31.
- (72) Rothman, L. S.; Jacquemart, D.; Barbe, A.; Benner, D. C.; Birk, M.; Brown, L. R.; Carleer, M. R.; Chackerian, J. C.; Chance, K.; Coudert, L. H.; Dana, V.; Devi, V. M.; Flaud, J.-M.; Gamache, R. R.; Goldman, A.; Hartmann, J.-M.; Jucks, K. W.; Maki, A. G.; Mandin, J.-Y.; Massie, S. T.; Orphal, J.; Perrin, A.; Rinsland, C. P.; Smith, M. A. H.; Tennyson, J.; Tolchenov, R. N.; Toth, R. A.; Auwera, J. V.; Varanasi, P.; Wagner, G. J. *Quant. Spectrosc. Radiat. Transfer* **2005**, 96, 139.
- (73) Wallington, T. J. Nielsen, O. J. in *Peroxy Radicals*; John Wiley and Sons: New York, 1997; Chap. 15.
- (74) Ahmed, M.; Blunt, D.; Chen, D.; Suits, A. G. *J. Chem. Phys.* **1997**, 106, 7617.
- (75) Baklanov, A. V.; Krasnoperov, L. N. *J. Phys. Chem. A* **2001**, 105, 97.
- (76) Frisch, M. J.; Trucks, G. W.; Schlegel, H. B.; Scuseria, G. E.; Robb, M. A.; Cheeseman, J. R.; Montgomery, J. A., Jr.; Vreven, T.; Kudin, K. N.; Burant, J. C.; Millam, J. M.; Iyengar, S. S.; Tomasi, J.; Barone, V.; Mennucci, B.; Cossi, M.; Scalmani, G.; Rega, N.; Petersson, G. A.; Nakatsuji, H.; Hada, M.; Ehara, M.; Toyota, K.; Fukuda, R.; Hasegawa, J.; Ishida, M.; Nakajima, T.; Honda, Y.; Kitao, O.; Nakai, H.; Klene, M.; Li, X.; Knox, J. E.; Hratchian, H. P.; Cross, J. B.; Bakken, V.; Adamo, C.; Jaramillo, J.; Gomperts, R.; Stratmann, R. E.; Yazyev, O.; Austin, A. J.; Cammi, R.; Pomelli, C.; Ochterski, J. W.; Ayala, P. Y.; Morokuma, K.; Voth, G. A.; Salvador, P.; Dannenberg, J. J.; Zakrzewski, V. G.; Dapprich, S.; Daniels, A. D.; Strain, M. C.; Farkas, O.; Malick, D. K.; Rabuck, A. D.; Raghavachari, K.; Foresman, J. B.; Ortiz, J. V.; Cui, Q.; Baboul, A. G.; Clifford, S.; Cioslowski, J.; Stefanov, B. B.; Liu, G.; Liashenko, A.; Piskorz, P.; Komaromi, I.; Martin, R. L.; Fox, D. J.; Keith, T.; Al-Laham, M. A.; Peng, C. Y.; Nanayakkara, A.; Challacombe, M.; Gill, P. M. W.; Johnson, B.; Chen, W.; Wong, M. W.; Gonzalez, C.; Pople, J. A. *Gaussian 03, revision B.05*; Gaussian, Inc., Wallingford, CT, 2004.
- (77) Cavallotti, C.; Rota, R.; Faravelli, T.; Ranzi, E. *Proc. Combust. Inst.* **2007**, 31, 201.
- (78) Computational Chemistry Comparison and Benchmark Database, <http://cccbdb.nist.gov/default.htm>.
- (79) Duschinsky, F. *Acta Physicochim. URSS* **1937**, 7, 551.
- (80) MolFC 2.3.4, <http://www.theochem.unisa.it/molfc.html>.
- (81) Borrelli, R.; Peluso, A. *J. Chem. Phys.* **2003**, 119, 8437.
- (82) Stanton, J. F. Private communication.

JP907605J